

Robust Remote Sensing Image–Text Retrieval with Noisy Correspondence

Qiya Song¹, Yiqiang Xie¹, Yuan Sun^{2*}, Renwei Dian³, Xudong Kang³

¹Hunan Normal University, Changsha, China 410081

²Sichuan University, Chengdu, China 610044

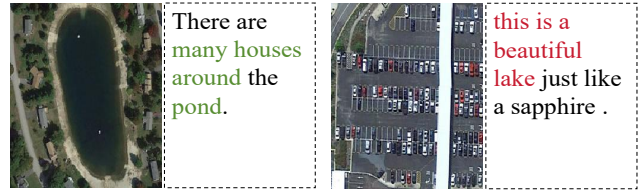
³Hunan University, Changsha, China 410082

sqyunb@hnu.edu.cn, yiqiang.xie@hunnu.edu.cn, sunyuan_work@163.com

Abstract

As a pivotal task that bridges remote visual and linguistic understanding, Remote Sensing Image–Text Retrieval (RSITR) has attracted considerable research interest in recent years. However, almost all RSITR methods implicitly assume that image–text pairs are matched perfectly. In practice, acquiring a large set of well-aligned data pairs is often prohibitively expensive or even infeasible. In addition, we also notice that the remote sensing datasets (e.g., RSITMD) truly contain some inaccurate or mismatched image text descriptions. Based on the above observations, we reveal an important but untouched problem in RSITR, i.e., Noisy Correspondence (NC). To overcome these challenges, we propose a novel Robust Remote Sensing Image–Text Retrieval (RRSITR) paradigm that designs a self-paced learning strategy to mimic human cognitive learning patterns, thereby learning from easy to hard from multi-modal data with NC. Specifically, we first divide all training sample pairs into three categories based on the loss magnitude of each pair, i.e., clean sample pairs, ambiguous sample pairs, and noisy sample pairs. Then, we respectively estimate the reliability of each training pair by assigning a weight to each pair based on the values of the loss. Further, we respectively design a new multi-modal self-paced function to dynamically regulate the training sequence and weights of the samples, thus establishing a progressive learning process. Finally, for noisy sample pairs, we present a robust triplet loss to dynamically adjust the soft margin based on semantic similarity, thereby enhancing the robustness against noise. Extensive experiments on three popular benchmark datasets demonstrate that the proposed RRSITR significantly outperforms the state-of-the-art methods, especially in high noise rates. The code is available at: <https://github.com/MSFLabX/RRSITR>.

*Corresponding authors.



(a) Perfect correspondence

(b) Noisy correspondence

Figure 1. Representative examples of noise correspondence problems that really exist in the RSITMD dataset, wherein the sample pair is erroneously assumed to be semantically aligned. Since the model lacks explicit knowledge of which sample pairs are noisy during training, such incorrect supervision signals inevitably weaken retrieval performance. (a) and (b) represent clean sample pairs and noisy mismatched ones, respectively.

1. Introduction

Remote Sensing Image–Text Retrieval (RSITR) [15, 28, 31, 37, 42] aims to bridge the semantic gap between aerial or satellite imagery and natural language descriptions, thereby enabling bidirectional querying, for example, retrieving relevant images given a textual query or retrieving descriptive captions for a given overhead scene. Thus, RSITR has attracted considerable research attention [34, 36, 41], which demonstrates significant application potential in various domains such as environmental monitoring [14], urban planning [32], and disaster assessment [10]. In recent years, numerous RSITR methods have been proposed, which could be primarily divided into two categories, i.e., Deep Convolutional Neural Network (DCNN) based methods and Transformer-based methods. The former employs convolutional neural networks and recurrent neural networks to extract and fuse image–text features for cross-modal retrieval. For instance, SIRS [43] achieves fine-grained alignment via semantic segmentation, while MSA [33] employs multi-scale alignment for richer representations. The latter utilizes separate Transformer branches for each modality and aligns features in a shared space. Representative works include RemoteCLIP [17], a foundation model trained with

large-scale data excelling in retrieval tasks.

Although these methods have achieved pleasing performance, they rely on the ideal assumption of perfectly aligned image-text pairs in training data. However, due to the predominantly nadir or vertical viewing geometry, remote sensing images lack human-centric egocentric visual priors (e.g., frontal or lateral views), leading to inherent ambiguity in text descriptions. Thus, constructing accurately the large scale of aligned remote sensing data is often prohibitively expensive and infeasible. As shown in Fig.1, the RSITMD dataset factually contains some inaccurate/mismatched textual descriptions. Although a few studies [9, 19, 22, 27] have noticed the existence of meaningless or weakly correlated image-text pairs, almost all methods have failed to explicitly reveal such noisy pairs. Based on the above observation, we reveal an important but untouched problem in RSITR, i.e., Noisy Correspondence (NC). These mismatched pairs would inevitably mislead the learning process of the model, weakening the cross-modal retrieval performance. The core challenge is how to endow neural networks with robustness against such noise, thereby alleviating the interference of NC.

To alleviate the negative effects caused by NC, we propose a novel Robust Remote Sensing Image-Text Retrieval (RRSITR) paradigm that simulates the human cognitive ability to enable progressive learning from easy to hard instances for noisy multi-modal data, as shown in Fig.2. Specifically, we first finely divide remote sensing data pairs into three groups according to the magnitude of loss, thereby enabling differentiated processing of the correspondence between clean, ambiguous, and noisy data. Then, we assign each pair a reliability weight derived from its loss value to achieve an adaptive assessment of its contribution to the learning process. Afterwards, for clean and ambiguous data, we design a new self-paced function to dynamically adjust both the weights and the learning sequence of the samples throughout training, thereby enabling the model to learn more semantic information from easy to hard. For noisy pairs, we propose a robust triplet loss to improve noise robustness by dynamically adjusting soft margins based on inter-sample semantic similarity. In summary, the main contributions of this work are as follows:

- We reveal and study a ubiquitous and untouched problem in RSITR, dubbed noisy correspondence (NC). To the best of our knowledge, this paper could be the first work to prevent the model from being misled by incorrect visual semantic associations.
- We propose a new multi-modal self-paced learning strategy to enable the model to learn from easy to hard in an organized manner for clean and ambiguous pairs. Moreover, we design a robust triplet loss to mitigate the adverse impact of NC.
- Extensive experiments on three benchmark datasets show

that our RRSITR significantly outperforms state-of-the-art methods, particularly in high noise scenarios.

2. Related Work

2.1. Remote Sensing Image-Text Retrieval

Remote Sensing Image-Text Retrieval (RSITR) aims to retrieve semantically relevant remote sensing images given a text query, or vice versa. The core of this task lies in mapping data from different modalities into a shared embedding space, where cross-modal retrieval matching is achieved by maximizing the similarity of positive samples and minimizing that of negative samples. In recent years, a large number of RSITR methods have been proposed [8, 22, 23, 35, 39, 43]. For example, AMFMN [35] proposes an asymmetric multimodal feature matching network to address the challenges posed by multi-scale features and redundant information in remote sensing images. However, AMFMN struggles to distinguish subtle differences in semantically similar descriptions. To address this, KAMCL [8] introduces a knowledge-assisted learning framework that enhances the model’s ability to discern fine-grained distinctions by leveraging discriminative information between similar descriptions. With the rapid development of vision-language pre-training models, some RSITR methods based on this paradigm have been proposed [1, 6, 9, 17, 29, 40]. For instance, as the first vision-language foundation model in remote sensing, RemoteCLIP [17] could significantly enhance remote sensing retrieval performance, though it encounters challenges associated with high computational resource consumption. To alleviate this issue, CUP [29] proposes a context and uncertainty-aware prompt network, significantly reducing resource overhead during model optimization. Although existing methods make considerable progress, they generally rely heavily on accurately paired remote sensing image-text data. However, in practical applications, constructing high-quality annotated datasets is not only costly and time-consuming but also inevitably leads to mismatched remote sensing image-text pairs. To address this, we reveal and study the NC problem in remote sensing image-text pairs and further propose a robust RSITR method to mitigate the negative impact of such NC on the retrieval performance.

2.2. Self-paced Learning

Inspired by the human cognitive learning process, self-paced learning (SPL) [12] is proposed with a core idea that involves training models using a curriculum progressing from easy to hard samples. For instance, to mitigate the issue of noise or outliers, SCSM [16] employs an SPL strategy to learn gradually based on sample difficulty. However, this method requires manually designed weighting functions, which introduces additional hyperparam-

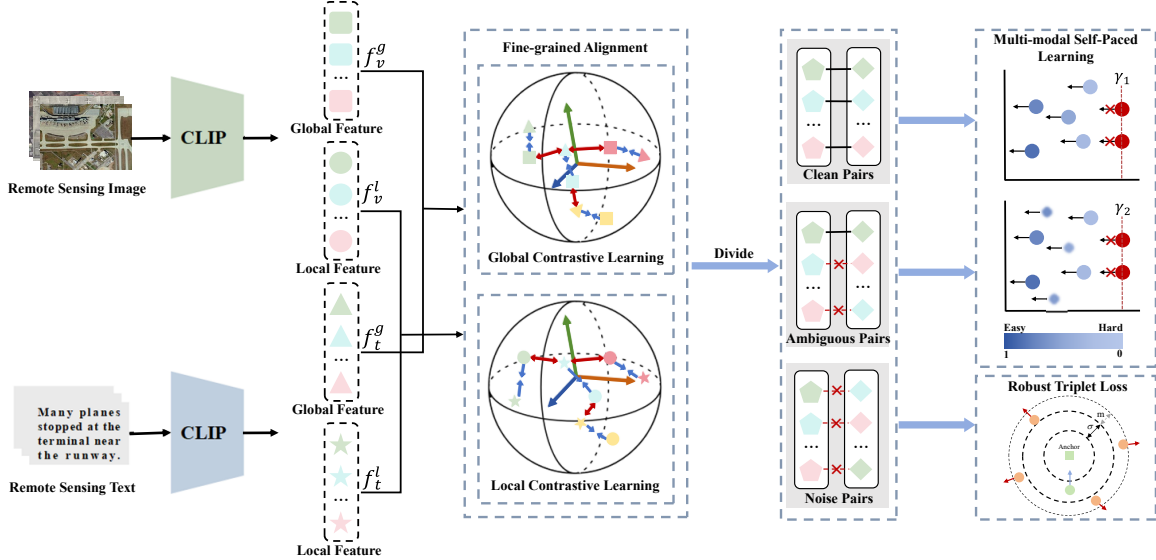


Figure 2. The overview of RRSITR. Specifically, we first achieve fine-grained alignment by both global and local contrastive learning. Based on contrastive loss magnitude, training pairs are categorized into clean, ambiguous, and noisy. A multimodal self-paced learning strategy then dynamically weights clean and ambiguous pairs, enabling progressive learning from easy to hard correspondences. For noisy pairs, a robust triplet loss enhances model robustness and retrieval performance.

ters and limits its applicability. To address this limitation, Meta-SPN [30] achieves automatic learning of weight values. Nevertheless, most existing methods primarily leverage an easy to hard learning strategy to counteract feature noise, yet they typically consider difficulty only at the instance level. In response, DSCMH [26] proposes an innovative dual-perspective self-paced learning mechanism that assesses difficulty from both instance-level and feature-level perspectives, thereby further enhancing model robustness. In contrast, DHaPH [7] places greater emphasis on hard sample pairs, assigning them larger weights to excavate discriminative information. Furthermore, RSHNL [25] focuses on handling multi-modal data with noisy labels to improve the noise robustness of hash models. Although these SPL approaches have achieved notable results, they predominantly address noise or outliers within the data. When dealing with remote sensing image-text data with NC, there remains a lack of research on leveraging SPL to mitigate the noisy correspondence problem.

3. Method

3.1. Problem Formulation

For clarity of presentation, in this paper, we define the image set $\mathcal{V} = \{I_i\}_{i=1}^{N_v}$ and the corresponding text set $\mathcal{T} = \{T_i\}_{i=1}^{N_t}$, where N_v and N_t representing the number of images and texts, respectively. The image-text pair is presented as $\mathcal{D} = \{(I_i, T_i, y_i)\}_{i=1}^N$, where each image I_i is associated with a text T_i . N represents the number of image-text pairs. $y_i \in \{0, 1\}$ represents the correspondence label, where $y_i = 1$ indicates the correct correspondence,

otherwise $y_i = 0$. Following [9], for the input image-text data $\{(I_i, T_i)\}$, we employ the CLIP visual encoder to extract its global visual feature f_v^g and local visual features $\{f_v^1, \dots, f_v^{d_1}\}$. For an input text T_i , we use the CLIP text encoder to extract its global text feature f_t^g and local text features $\{f_t^1, \dots, f_t^{d_2}\}$. The above process could be formulated as:

$$\begin{aligned} f_v^g, f_v^1 \dots f_v^{d_1} &= \varphi(I_i), \\ f_t^g, f_t^1 \dots f_t^{d_2} &= \phi(T_i), \end{aligned} \quad (1)$$

where φ and ϕ are the CLIP visual encoder and the CLIP text encoder, respectively. d_1 and d_2 are the number of local visual features and local text features, respectively.

3.2. Fine-grained Alignment

To achieve more precise cross-modal alignment between images and texts, we propose a fine-grained alignment scheme to leverage both global information and local details. Specifically, we first calculate the global similarity of each image-text pair by the cosine similarity, i.e.,

$$S^g = \cos(f_v^g, f_t^g). \quad (2)$$

Afterwards, we compute the local similarity of each local block $S_{ij}^l = \cos(f_v^i, f_t^j)$. Then, we compute the local similarity of each image-text pair by performing two consecutive L2-norm operations, i.e.,

$$S^l = \|S_{ij}^l\|_{2,2}, \quad (3)$$

where $\|\cdot\|_{2,2}$ represents two consecutive L2-norm.

To achieve the fine-grained alignment of multi-modal data, we adopt the InfoNCE loss [21] to maximize the similarities of positive pairs while minimizing the similarities of

the negative pairs, which could be defined as:

$$\begin{aligned}\mathcal{L}_{info}^g &= -\frac{1}{N} \sum_{j=1}^N \left(\log \frac{\exp(S_{jj}^g/\tau)}{\sum_{i=1}^N \exp(S_{ji}^g/\tau)} + \log \frac{\exp(S_{jj}^g/\tau)}{\sum_{i=1}^N \exp(S_{ij}^g/\tau)} \right), \\ \mathcal{L}_{info}^l &= -\frac{1}{N} \sum_{j=1}^N \left(\log \frac{\exp(S_{jj}^l/\tau)}{\sum_{i=1}^N \exp(S_{ji}^l/\tau)} + \log \frac{\exp(S_{jj}^l/\tau)}{\sum_{i=1}^N \exp(S_{ij}^l/\tau)} \right),\end{aligned}\quad (4)$$

where S_{jj}^g and S_{jj}^l denote the j -th global and local positive sample pairs, respectively. $\sum_{i=1}^N S_{ji}^g$ and $\sum_{i=1}^N S_{ji}^l$ represent the row-wise sums of the similarity matrices for image-to-text alignment. $\sum_{i=1}^N S_{ij}^g$ and $\sum_{i=1}^N S_{ij}^l$ represent the row-wise sums of the similarity matrices for text-to-image alignment. τ denotes the temperature hyperparameter, and N denotes the batch size. Finally, we apply the InfoNCE loss to achieve both global and local alignment, which could be expressed as:

$$\mathcal{L}_{info}^{gl} = \mathcal{L}_{info}^g + \mathcal{L}_{info}^l, \quad (5)$$

where \mathcal{L}_{info}^g is the global contrastive loss and \mathcal{L}_{info}^l is the local contrastive loss.

3.3. Multi-modal Self-Paced Learning

Inspired by the human cognitive process of learning from easy to hard, we propose a multi-modal self-paced learning scheme to mitigate the interference of NC during the training. Specifically, RRSITR dynamically partitions all training sample pairs into three subsets, i.e., clean sample pairs, ambiguous sample pairs, and noisy sample pairs, based on their total contrastive loss values. For samples of different qualities, we design a self-paced weighting function to dynamically assess sample difficulty and control their participation order and contribution during training. The model is trained to first learn from simple and reliable clean samples along with ambiguous samples, then gradually incorporate more challenging ones. This progressive curriculum learning strategy enables the model to steadily capture the alignment between images and texts, thereby effectively suppressing the negative impact of incorrect correspondences and enhancing overall robustness. RRSITR dynamically adjusts the participation manner and weight of sample pairs based on the relationship between the current loss ℓ_i and thresholds γ_1, γ_2 .

When $\ell_i < \gamma_1$, clean sample pairs are deemed reliable and easy to learn. RRSITR incorporates these samples in the early stages of training and gradually introduces more challenging ones. When $\gamma_1 \leq \ell_i < \gamma_2$, ambiguous pairs are considered relatively reliable but exhibit some degree of difficulty. RRSITR prioritizes the learning of these samples. The loss functions for these samples are defined as:

$$\begin{aligned}\mathcal{L}_{S1} &= \frac{1}{N} \sum_{i=1}^N w_i \underbrace{(\mathcal{L}_i^g + \mathcal{L}_i^l)}_{\ell_i} + \frac{1}{N} \sum_{i=1}^N \mathcal{R}(w_i, \gamma_1), \\ \mathcal{L}_{S2} &= \frac{1}{N} \sum_{i=1}^N w_i \underbrace{(\mathcal{L}_i^g + \mathcal{L}_i^l)}_{\ell_i} + \frac{1}{N} \sum_{i=1}^N \mathcal{R}(w_i, \gamma_2),\end{aligned}\quad (6)$$

where ℓ_i denotes the sum of the global contrastive loss and the local contrastive loss for the i -th sample pair, $w_i \in [0, 1]$ denotes the importance weight of the i -th sample pair, assessing its reliability, and $\mathcal{R}(w_i, \gamma)$ is a self-paced regularizer governed by the learning pace parameter γ , assigning a weight w_i to each sample based on its learning difficulty.

When $\ell_i \geq \gamma_2$, the sample pairs are considered potentially noisy correspondence. Thus, the weight w_i is set to zero to exclude it from training. In summary, RRSITR simulates the human cognitive learning process that progresses from easy to hard, gradually incorporating more sample pairs into the model training.

To achieve finer control over the sample selection strategy and training progress for more robust learning with noisy correspondence, we design a novel self-paced regularizer $\mathcal{R}(w_i, \gamma)$, expressed as follows:

$$\mathcal{R}(w_i, \gamma) = \begin{cases} -\frac{2}{\pi} \gamma [w_i \arccos(w_i) - \sqrt{1-w_i^2}], & \ell_i < \gamma, \\ 0, & \ell_i \geq \gamma. \end{cases} \quad (7)$$

In general, the weight could be viewed as an indicator of the easiness for each noisy pair. A higher weight suggests the instance is simpler. As the learning process proceeds, the loss gradually decreases, thereby increasing the weight.

3.4. Robust Triplet Loss

The hard triplet loss is a widely adopted metric learning objective in cross-modal representation learning [4, 5, 13, 24, 38]. It enforces semantic alignment by encouraging the similarity between a positive cross-modal pair to exceed that of negative pairs by a margin. Hard triplet loss achieves strong empirical performance by leveraging hard negative mining, particularly the hardest negatives within each mini-batch. However, in the presence of noisy data, positive sample pairs may be incorrectly matched, resulting in a low similarity score $S^g(\mathbf{v}_i, \mathbf{t}_i)$. Under such circumstances, the difference between the positive sample similarity and the hardest negative sample similarity often increases, thereby expanding the margin and forcing the model to distinguish between positive and negative samples with stricter standards, effectively suppressing noise interference. In contrast, fixed-margin methods often lead the model to become overconfident on easy samples while underlearning hard samples. For noisy pairs, we propose a Robust Triplet Loss (RTL) to further enhance robustness against NC through an adaptive margin mechanism and a hard sample mining strategy. The loss function could be written as follows:

$$\begin{aligned}\mathcal{L}_{soft} &= \frac{1}{N} \sum_{i=1}^N ([\hat{\mu}_i - S^g(\mathbf{v}_i, \mathbf{t}_i) + S^g(\mathbf{v}_i, \hat{\mathbf{t}}_h)]_+ \\ &\quad + [\hat{\zeta}_i - S^g(\mathbf{v}_i, \mathbf{t}_i) + S^g(\hat{\mathbf{v}}_h, \mathbf{t}_i)]_+),\end{aligned}\quad (8)$$

where $S^g(\mathbf{v}_i, \mathbf{t}_i)$ denotes the global similarity of positive sample pairs and $[x]_+ \equiv \max(x, 0)$. Here, $\hat{\mathbf{v}}_h = \arg \max_{v_j \neq v_i} S^g(v_j, \mathbf{t}_i)$ and $\hat{\mathbf{t}}_h = \arg \max_{t_j \neq t_i} S^g(\mathbf{v}_i, t_j)$

are the most similar negatives to t_i and v_i in a batch. The soft margins $\hat{\mu}_i$ and $\hat{\zeta}_i$ are adaptively determined as follows:

$$\begin{aligned}\hat{\mu}_i &= \sigma * (1 + \max(0, S^g(\mathbf{v}_i, \hat{\mathbf{t}}_h) - S^g(\mathbf{v}_i, \mathbf{t}_i))), \\ \hat{\zeta}_i &= \sigma * (1 + \max(0, S^g(\hat{\mathbf{v}}_h, \mathbf{t}_i) - S^g(\mathbf{v}_i, \mathbf{t}_i))),\end{aligned}\quad (9)$$

where $\sigma > 0$ is a base margin hyperparameter. Through dynamic margin adjustment, RTL balances the learning focus, preventing the model from overfitting on noisy data. Furthermore, the bidirectional symmetric treatment in the loss function ensures that noise in both modalities can be covered by the adaptive margin mechanism, enhancing overall robustness and image-text consistency.

3.5. Overall Objective and Inference

The overall objective of our RRSITR is defined as follows:

$$\mathcal{L}_{overall} = \mathcal{L}_{S1} + \lambda_1 \mathcal{L}_{S2} + \lambda_2 \mathcal{L}_{soft}, \quad (10)$$

where λ_1 and λ_2 are the balancing factors. Due to the limited space, we attach the detailed training process is provided in the supplementary materials.

In the inference stage, to obtain a more fine-grained similarity relationship, we adopt a weighted scheme to fuse the global and local similarities, thereby obtaining the fine-grained image-text similarity S^f as follows:

$$S^f = \alpha S^g + (1 - \alpha) S^l, \quad (11)$$

where α is a hyperparameter.

3.6. Weight Analysis

To solve the minimization problem in Equation (6), we conduct a thorough analysis of how the weights w_i influence the loss function \mathcal{L}_S . Specifically, we alternately update the weight w_i and the network parameter Θ to minimize \mathcal{L}_S . Under the condition of the fixed Θ , the optimal solution of the weight w_i could be written as:

$$w_i = \begin{cases} \underset{w_i \in [0,1]}{\operatorname{argmin}} \left\{ w_i \ell_i - \frac{2}{\pi} \gamma \left[w_i \arccos(w_i) - \sqrt{1-w_i^2} \right] \right\}, & \ell_i < \gamma, \\ 0, & \ell_i \geq \gamma. \end{cases} \quad (12)$$

When $\ell_i - \gamma < 0$, let the derivative of Equation (12) to zero, we can obtain:

$$w_i^* = \cos \left(\frac{\pi}{2} \cdot \frac{\ell_i}{\gamma} \right). \quad (13)$$

Given that $\gamma \geq 0$ and $\ell_i \geq 0$, it can be derived that $w_i \in [0, 1]$. Thus, the optimal weight solution is expressed as follows:

$$w_i^* = \begin{cases} \cos \left(\frac{\pi}{2} \cdot \frac{\ell_i}{\gamma} \right), & \ell_i < \gamma, \\ 0, & \ell_i \geq \gamma. \end{cases} \quad (14)$$

When the loss value ℓ_i is excessively large (i.e., $\ell_i \geq \gamma$), the corresponding sample pairs are treated as hard data with noisy correspondences and are assigned a weight of zero. When $\ell_i < \gamma$, the i -th sample pair with larger weight is implicitly regarded as easy, whereas those with smaller weights are regarded as hard. Overall, this strategy not only effectively distinguishes noise pairs but also enhances the model’s robustness and generalization capability.

4. Experiments

4.1. Datasets

In our experiments, to validate the effectiveness of the proposed method, we employ three benchmark datasets, i.e., RSITMD [35], RSICD [18], and NWPU [2]. Following the protocol in [39], we split each dataset into 80% for training, 10% for validation, and 10% for testing, respectively. To simulate real-world misalignment scenarios, we introduce synthetic noise into the training set by randomly shuffling text descriptions across images, thereby generating controlled NC. We employ four noise rates (i.e., 20%, 40%, 60%, and 80%) to evaluate model robustness under varying degrees of correspondence degradation. Dataset details and experimental results of 0% noise rate are shown in supplementary materials¹.

4.2. Implementation Details

The RRSITR method adopts the ViT-B-32 architecture provided by OpenCLIP [3] as the backbone network. The model is trained using the Adam optimizer [11] for 50 epochs with a batch size of 100. We adopt a linear warm-up and cosine learning rate scheduler. Moreover, the learning rate, weight decay, warmup steps, and the maximum gradient norm are set to $7e^{-6}$, 0.7, 200, and 50, respectively. For some parameters, we set γ_1 , γ_2 , σ , λ_1 , λ_2 , and α to 5, 18, 0.6, 0.8, 0.9, and 0.9 on all datasets. All experiments are implemented based on PyTorch and trained on a single NVIDIA A800 GPU.

4.3. Comparison Methods

We compare the proposed RRSITR with some state-of-the-art methods, including SIRS [43], MSA [33], AMFMN [35], HVSA [39], SWAN [23], PIR [22], and KAMCL [8], S-CLIP [20], SEMICLIP [6], and CUP [29]. More details are shown in the supplementary materials. For all experiments, we utilize Rank at k (R@k, k=1,5,10) and mean Rank (mR) as the evaluation metrics to evaluate the retrieval performance [23]. Specifically, R@k measures the percentage of ground truth instances within the top R@k samples, while mR represents the average value across all R@k metrics, providing an overall assessment of retrieval performance. In our experiments, we select the best checkpoint according to validation performance. For fairness, we run five times using the recommended settings to record the mean scores and the standard deviation. For all experimental results, the highest scores and the second-highest scores are highlighted in **bold** and underlines, respectively.

4.4. Comparison with the State-of-the-Art Methods

Experimental results on the three datasets are reported in Tab.1, Tab.2, and Tab.3, respectively. From these results,

¹<https://github.com/MSFLabX/RRSITR>

Table 1. Image-text retrieval performance under different noise ratios on the RSITMD dataset.

Noise	Method	Ref.	Image-to-Text Retrieval			Text-to-Image Retrieval			mR
			R@1	R@5	R@10	R@1	R@5	R@10	
20%	AMFMN	TGRS'22	9.56±1.17	26.90±2.02	39.29±1.96	7.66±0.78	31.19±0.49	51.42±0.94	27.67±0.93
	HVSA	TGRS'23	7.87±0.99	23.54±1.52	34.87±2.72	6.35±0.29	27.57±0.71	47.46±1.03	24.61±0.74
	KAMCL	TGRS'23	10.80±0.89	27.17±1.08	39.87±1.32	9.59±0.61	34.04±0.65	51.23±1.15	28.78±0.76
	SWAN	ICMR'23	9.29±2.28	24.25±1.38	37.43±2.55	7.44±0.45	30.93±0.84	52.71±0.92	27.01±0.81
	PIR	ACMMM'23	10.09±1.66	29.25±1.69	44.95±1.19	8.74±0.89	33.45±1.25	54.04±1.06	30.09±0.89
	S-CLIP	NeurIPS'23	6.99±0.86	25.66±0.31	41.06±1.98	6.90±1.01	24.87±2.68	38.85±1.60	24.05±1.20
	SIRS	TGRS'24	10.13±0.68	28.27±0.87	40.84±0.89	7.70±0.62	32.30±0.78	52.87±0.78	28.69±0.14
	MSA	TGRS'24	12.88±0.88	31.33±1.46	45.49±2.33	10.11±0.28	38.14±1.48	57.64±0.83	32.60±0.54
	SEMICLIP	ICLR'25	8.40±1.15	27.98±0.83	42.48±1.70	7.34±1.50	28.58±2.03	45.10±1.71	26.65±1.13
	CUP	TNNLS'25	19.78±0.64	38.94±2.30	52.52±1.28	15.30±1.10	44.64±1.53	62.73±0.97	38.99±1.16
	RRSITR	Ours	24.60±1.38	46.68±1.11	58.85±1.92	20.19±0.89	53.04±0.70	70.12±0.37	45.58±0.38
40%	AMFMN	TGRS'22	7.30±0.73	21.72±0.81	33.89±2.03	6.13±0.67	27.04±0.83	45.60±0.84	23.61±0.60
	HVSA	TGRS'23	6.33±0.72	18.36±1.20	28.80±2.48	4.85±0.31	19.87±0.98	36.48±1.81	19.12±1.08
	KAMCL	TGRS'23	5.62±2.37	16.24±6.38	26.10±9.99	4.99±1.68	20.03±5.83	33.12±7.94	17.68±5.55
	SWAN	ICMR'23	7.26±0.80	22.39±0.65	35.53±0.55	6.27±0.17	27.80±0.65	48.71±1.53	24.66±0.40
	PIR	ACMMM'23	7.66±0.83	24.87±1.47	37.43±0.95	6.74±0.53	29.10±0.91	50.82±0.42	26.10±0.50
	S-CLIP	NeurIPS'23	3.36±1.45	12.70±4.86	20.97±8.01	3.05±1.49	11.33±5.65	19.82±8.69	11.87±4.99
	SIRS	TGRS'24	7.66±0.89	22.61±0.53	35.35±1.05	5.97±0.64	26.86±0.79	44.85±0.85	23.88±0.51
	MSA	TGRS'24	3.54±0.90	12.08±2.98	21.11±4.79	5.24±0.62	22.35±2.23	37.53±3.41	16.98±2.06
	SEMICLIP	ICLR'25	6.19±1.15	21.59±1.24	34.11±1.12	6.09±0.83	22.10±1.87	34.52±2.00	20.77±1.24
	CUP	TNNLS'25	17.97±0.60	37.25±1.07	51.19±0.87	13.72±0.69	40.91±0.72	59.35±0.35	36.73±0.26
	RRSITR	Ours	23.23±1.53	43.63±0.43	56.15±0.38	19.27±0.88	51.09±1.10	68.48±0.64	43.64±0.28
60%	AMFMN	TGRS'22	6.46±1.04	20.27±1.56	31.28±1.80	5.20±1.03	21.76±1.20	37.33±1.72	20.38±1.02
	HVSA	TGRS'23	4.78±0.48	14.20±1.59	22.92±1.69	3.17±0.69	15.79±1.05	27.21±1.09	14.68±0.71
	KAMCL	TGRS'23	0.44±0.24	1.73±0.86	3.59±1.42	0.59±0.28	3.15±1.45	5.96±2.57	2.58±0.80
	SWAN	ICMR'23	6.42±0.89	19.43±1.17	32.17±0.92	5.51±0.08	24.27±0.97	43.62±1.26	21.90±0.57
	PIR	ACMMM'23	7.39±1.12	23.10±0.89	36.68±1.08	5.38±0.62	25.46±0.85	46.23±1.15	24.04±0.66
	S-CLIP	NeurIPS'23	0.71±0.38	2.74±0.75	4.33±1.09	0.40±0.16	2.30±0.86	3.94±0.88	2.40±0.56
	SIRS	TGRS'24	6.24±0.36	19.56±0.82	29.82±0.96	4.24±0.29	18.37±0.45	31.41±0.49	18.27±0.15
	MSA	TGRS'24	0.26±0.09	1.64±0.55	3.32±0.81	1.68±0.32	7.58±0.44	14.50±1.46	4.83±0.50
	SEMICLIP	ICLR'25	3.89±0.69	13.41±1.73	21.25±2.80	3.23±0.63	12.87±1.98	21.17±2.23	12.64±1.45
	CUP	TNNLS'25	15.62±0.65	34.25±1.86	48.14±1.32	11.65±0.73	37.37±2.00	55.06±2.66	33.68±0.83
	RRSITR	Ours	22.03±0.59	41.50±1.60	54.20±1.06	17.72±0.66	49.63±0.81	67.30±0.63	42.06±0.28
80%	AMFMN	TGRS'22	3.50±0.26	13.54±0.68	20.89±1.23	3.69±0.35	13.81±0.59	24.61±0.31	13.34±0.47
	HVSA	TGRS'23	2.83±0.69	8.85±1.24	14.56±1.34	1.90±0.24	8.02±0.51	14.44±0.70	8.43±0.55
	KAMCL	TGRS'23	0.35±0.18	1.02±0.46	2.16±0.45	0.46±0.15	1.79±0.21	3.37±0.35	1.53±0.17
	SWAN	ICMR'23	3.23±1.39	12.08±1.89	20.80±0.90	3.33±0.48	14.34±1.37	26.16±1.78	13.32±1.10
	PIR	ACMMM'23	3.67±0.72	13.63±1.69	23.41±1.72	2.58±0.25	12.18±0.28	22.03±0.74	12.92±0.66
	S-CLIP	NeurIPS'23	0.26±0.16	1.50±0.47	2.70±0.33	0.26±0.16	1.24±0.41	2.65±0.75	1.44±0.30
	SIRS	TGRS'24	3.18±0.57	10.31±0.97	17.03±1.96	2.31±0.42	9.35±0.56	15.87±0.71	9.68±0.71
	MSA	TGRS'24	0.26±0.09	1.28±0.72	2.56±0.57	0.86±0.29	3.74±0.49	7.51±0.89	2.70±0.20
	SEMICLIP	ICLR'25	1.16±0.44	5.17±1.10	8.75±1.61	1.39±0.65	5.50±1.15	8.80±1.04	5.13±0.92
	CUP	TNNLS'25	10.71±0.75	27.61±1.43	40.35±1.38	8.27±0.78	30.38±1.47	48.22±2.67	27.59±0.99
	RRSITR	Ours	16.90±1.49	33.98±1.84	46.82±1.75	13.72±1.12	42.70±1.08	61.47±0.69	35.93±0.68

we could observe that: 1) The RRSITR method demonstrates comprehensively leading performance and exceptional noise robustness across all three datasets. 2) As the noise rate increases sharply from 20% to 80%, the retrieval performance of all baseline methods declines substantially on the datasets with synthetic NC. However, our RRSITR maintains relatively high performance, with its stability far surpassing other methods under the extreme noise scenario (i.e., 80%). 3) In specific retrieval tasks, RRSITR achieves the highest scores on key metrics such as R@1, which stems from its cognitive learning strategy. Our RRSITR could effectively avoid the misleading of noisy pairs and enhance the distinction between positive and negative sample pairs.

4.5. Ablation Studies

To investigate the role of each component in our RRSITR, ablation studies are conducted on the RSITMD dataset with an 80% noise ratio. More ablation studies are provided in the supplementary materials. We compare the proposed RRSITR with eight variants. Specifically, #1, #2, #3, and #4 represent the removal of the local contrastive learning mod-

ule, SPL module, RTL module, and all components, respectively. To further validate the SPL and RTL modules, we replace the SPL module in RRSITR with #5 (SPL with hard to easy strategy), #6 (SPL with random sample weighting) and #7 (SPL with ambiguous category removal). Meanwhile, #8 is defined by replacing the RTL module with fixed margin triplet loss. As shown in Tab.4, we could obtain the following conclusion: 1) The complete RRSITR framework achieves the best overall performance under the 80% noise condition, demonstrating the efficacy of each component. 2) The synergistic interactions among modules significantly enhance model robustness, effectively addressing noisy correspondence challenges. 3) Both the proposed multi-modal SPL and RTL maintain remarkable performance at the 80% noise level, verifying their effectiveness and robustness in noisy environments.

4.6. Self-paced Behavior Analysis

To investigate the adaptive learning behavior of our proposed RRSITR model, we draw the density distribution of sample weights from different training epochs on the

Table 2. Image-text retrieval performance under different noise ratios on the RSICD dataset.

Noise	Method	Ref.	Image-to-Text Retrieval			Text-to-Image Retrieval			mR
			R@1	R@5	R@10	R@1	R@5	R@10	
20%	AMFMN	TGRS'22	4.68±0.33	15.08±0.48	24.99±1.12	4.08±0.10	16.31±0.64	27.65±0.83	15.47±0.34
	HVSA	TGRS'23	4.76±0.40	14.93±0.69	25.21±1.33	2.85±0.29	13.15±0.67	24.85±1.00	14.29±0.49
	KAMCL	TGRS'23	7.59±0.79	20.48±0.57	31.31±0.41	5.75±0.23	21.38±0.46	34.70±0.66	20.20±0.28
	SWAN	ICMR'23	4.50±0.62	13.76±0.82	22.71±1.04	3.45±0.21	15.43±0.85	28.54±0.69	14.73±0.25
	PIR	ACMMM'23	7.36±0.38	20.29±0.64	31.64±1.46	5.41±0.32	20.68±0.32	34.84±0.85	20.04±0.50
	S-CLIP	NeurIPS'23	3.82±0.27	14.84±1.39	26.26±1.16	3.90±0.33	15.13±1.22	27.19±1.20	15.19±0.67
	SIRS	TGRS'24	4.80±0.44	14.38±1.06	24.17±1.04	3.48±0.14	16.11±0.51	29.41±0.64	15.39±0.52
	MSA	TGRS'24	6.99±0.65	20.28±0.81	31.77±0.90	5.65±0.33	21.93±0.44	37.12±0.49	20.62±0.18
	SEMICLIP	ICLR'25	4.85±0.49	17.59±0.45	29.24±1.03	4.28±0.83	17.13±0.80	28.54±0.86	16.94±0.58
	CUP	TNNLS'25	9.51±1.09	29.29±1.05	44.01±1.45	7.45±0.44	26.82±0.83	42.29±0.94	26.56±0.90
RRSITR	Ours	16.56±1.00	34.80±1.53	48.01±1.41	12.50±0.62	34.22±1.61	50.12±1.98	32.70±1.30	
40%	AMFMN	TGRS'22	3.68±0.40	13.03±0.71	21.67±0.95	3.09±0.15	12.95±0.42	23.62±1.00	13.01±0.10
	HVSA	TGRS'23	3.47±0.30	13.32±0.51	22.16±0.96	1.82±0.30	9.84±0.32	18.34±0.35	11.49±0.22
	KAMCL	TGRS'23	3.49±0.74	10.50±1.55	17.80±1.59	2.41±0.66	11.11±2.00	21.06±2.91	11.06±1.32
	SWAN	ICMR'23	3.31±0.40	10.67±0.45	19.87±0.64	2.97±0.27	13.23±0.79	25.49±1.16	12.59±0.27
	PIR	ACMMM'23	4.61±0.10	14.99±0.79	24.67±0.64	3.80±0.38	16.48±0.29	29.53±0.44	15.68±0.25
	S-CLIP	NeurIPS'23	3.09±0.60	12.31±1.60	21.17±1.95	2.85±0.51	11.47±1.50	20.70±2.70	11.93±1.25
	SIRS	TGRS'24	3.28±0.34	11.36±0.37	20.38±1.00	2.90±0.24	13.14±0.68	24.07±0.36	12.52±0.41
	MSA	TGRS'24	2.19±0.46	7.63±1.59	13.83±2.14	3.27±0.33	14.04±0.56	26.00±1.16	11.16±0.96
	SEMICLIP	ICLR'25	3.66±0.32	13.70±0.94	22.58±1.02	2.91±0.62	11.91±1.02	20.62±1.50	12.56±0.77
	CUP	TNNLS'25	9.11±0.83	28.16±1.24	42.16±1.57	7.33±0.32	24.83±0.73	39.63±0.97	25.20±0.59
RRSITR	Ours	15.77±0.70	34.15±0.42	47.36±1.53	11.81±0.88	35.09±0.65	50.90±1.38	32.51±0.63	
60%	AMFMN	TGRS'22	3.44±0.55	10.87±0.62	18.87±1.41	2.49±0.27	10.75±0.67	19.29±1.41	10.95±0.56
	HVSA	TGRS'23	3.50±0.19	12.42±0.45	20.88±0.83	1.72±0.12	8.37±0.22	15.49±0.45	10.40±0.21
	KAMCL	TGRS'23	0.79±0.62	2.56±1.95	5.23±3.83	0.87±0.23	4.38±1.36	8.45±2.84	3.71±1.75
	SWAN	ICMR'23	2.80±0.21	8.84±1.04	16.72±1.93	2.82±0.28	12.88±0.65	23.95±0.98	11.34±0.41
	PIR	ACMMM'23	3.35±0.62	10.65±1.23	18.63±0.57	2.79±0.28	12.60±0.80	23.06±0.97	11.85±0.65
	S-CLIP	NeurIPS'23	0.46±0.28	1.85±0.68	3.40±0.69	0.16±0.10	1.10±0.32	2.32±0.79	1.55±0.42
	SIRS	TGRS'24	2.32±1.16	7.10±3.62	13.63±6.55	1.65±0.83	8.03±3.83	15.31±7.12	8.01±3.82
	MSA	TGRS'24	0.14±0.07	0.40±0.08	0.69±0.12	1.07±0.23	4.62±0.57	8.67±0.96	2.60±0.28
	SEMICLIP	ICLR'25	2.34±0.22	9.28±0.38	16.14±0.54	1.70±0.21	8.69±0.71	15.09±0.78	8.87±0.32
	CUP	TNNLS'25	7.21±0.81	24.58±0.80	38.61±1.03	6.21±0.57	22.51±1.63	36.34±1.71	22.58±0.88
RRSITR	Ours	15.75±0.85	33.91±0.43	47.28±0.95	11.92±0.71	33.81±0.91	49.23±1.36	31.98±0.57	
80%	AMFMN	TGRS'22	2.51±0.47	8.97±0.79	16.27±0.54	1.88±0.12	8.67±0.32	16.08±0.37	9.06±0.26
	HVSA	TGRS'23	1.98±0.22	8.91±0.56	15.33±1.26	0.96±0.10	5.02±0.44	9.43±0.91	6.94±0.48
	KAMCL	TGRS'23	0.11±0.04	0.25±0.04	0.51±0.09	0.09±0.00	0.45±0.06	1.00±0.14	0.40±0.05
	SWAN	ICMR'23	1.74±0.42	6.00±0.77	11.60±1.29	1.67±0.22	8.11±0.38	15.54±0.55	7.44±0.56
	PIR	ACMMM'23	2.49±0.50	9.57±0.78	18.41±1.39	2.10±0.12	10.80±0.80	20.46±0.97	10.64±0.59
	S-CLIP	NeurIPS'23	0.18±0.12	0.77±0.15	1.37±0.34	0.13±0.04	0.53±0.10	1.02±0.14	0.67±0.14
	SIRS	TGRS'24	1.86±0.34	6.13±0.57	11.18±0.89	1.11±0.05	5.15±0.28	9.57±0.47	5.83±0.38
	MSA	TGRS'24	0.09±0.00	0.46±0.13	0.73±0.15	0.31±0.10	1.84±0.10	3.31±0.34	1.12±0.10
	SEMICLIP	ICLR'25	1.21±0.17	4.37±0.84	7.67±0.96	0.82±0.39	4.12±1.01	7.12±1.68	4.22±0.78
	CUP	TNNLS'25	5.87±0.56	20.93±0.36	34.33±0.82	5.51±0.37	19.70±0.93	32.59±1.14	19.82±0.45
RRSITR	Ours	13.47±0.90	28.80±1.47	41.41±1.81	10.02±1.04	30.55±1.70	45.13±1.93	28.23±1.26	

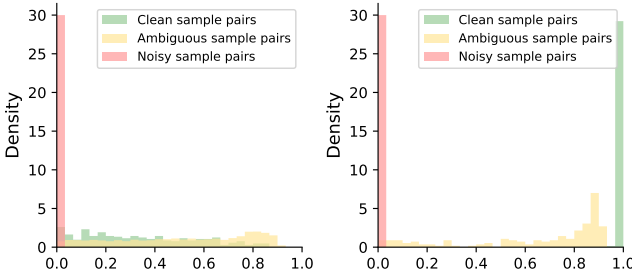


Figure 3. Density versus weight of all sample pairs on RSITMD during training at the 1st epoch (left) and the 50th epoch (right).

RSITMD dataset under a 40% noise rate. As shown in Fig.3, during the initial training phase, the RRSITR model first assigns zero weights to hard samples, treating them as noisy pairs. Thus, in the early stages of training, we can only better identify noisy pairs. As training progresses, we can effectively divide the training data into three subsets, i.e., clean, ambiguous, and noisy data. Our RRSITR gradually learns all clean and ambiguous samples from easy to hard, thereby enhancing its ability to distinguish noisy sam-

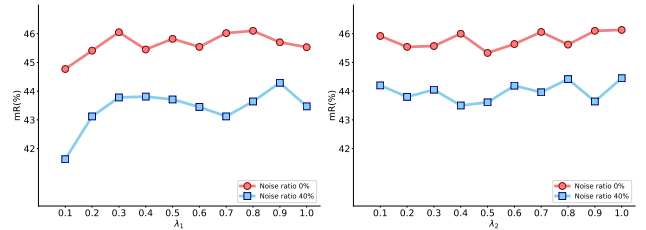


Figure 4. Parameters analysis (i.e., λ_1 and λ_2) on RSITMD.

ples and improving the model's robustness to NC.

4.7. Parameter Analysis

This study investigates the effects of λ_1 and λ_2 on retrieval performance. More parameter experiments in the supplementary materials. As shown in Fig.4, too large or too small parameters will lead to poor performance. Specifically, we could observe that the model maintains satisfactory performance in both noisy and noise-free environments when λ_1 lies in the range of 0.7 to 0.9 and λ_2 lies in the range of 0.7 to 1.0. This demonstrates that such a parameter combination effectively balances the contributions of the self-paced

Table 3. Image-text retrieval performance under different noise ratios on the NWPU dataset.

Noise	Method	Ref.	Image-to-Text Retrieval			Text-to-Image Retrieval			mR
			R@1	R@5	R@10	R@1	R@5	R@10	
20%	AMFMN	TGRS'22	5.47±0.24	21.99±0.79	36.89±0.73	4.47±0.24	18.66±0.23	31.97±0.32	19.91±0.38
	HVSA	TGRS'23	2.80±0.34	10.97±0.34	19.92±0.50	1.68±0.07	7.96±0.20	15.50±0.17	9.81±0.18
	KAMCL	TGRS'23	14.01±0.47	43.13±0.61	60.81±0.67	9.12±0.15	30.40±0.29	46.23±0.36	33.95±0.34
	SWAN	ICMR'23	2.42±0.20	11.43±0.59	20.98±0.41	2.72±0.12	11.85±0.23	21.69±0.49	11.85±0.20
	PIR	ACMMM'23	10.61±0.30	37.13±0.88	56.07±0.47	7.55±0.20	27.57±0.24	43.30±0.32	30.37±0.30
	S-CLIP	NeurIPS'23	2.73±0.13	11.85±0.47	21.19±0.58	2.86±0.14	11.77±0.48	21.19±0.53	11.93±0.28
	SIRS	TGRS'24	2.76±0.28	11.84±0.87	21.54±0.37	2.22±0.09	10.59±0.22	19.65±0.19	11.43±0.23
	MSA	TGRS'24	6.46±0.35	24.39±0.90	40.02±0.94	6.69±0.22	24.96±0.61	40.33±0.89	23.81±0.47
	SEMICLIP	ICLR'25	5.66±0.48	16.81±0.54	28.81±0.70	4.43±0.23	17.26±0.71	29.41±0.49	17.06±0.37
	CUP	TNNLS'25	9.26±1.21	29.36±2.47	44.46±3.66	5.49±0.38	19.97±2.02	32.69±2.76	23.54±2.05
RRSITR	Ours	22.84±0.38	57.21±0.71	74.32±0.34	13.62±0.27	38.89±0.39	54.62±0.46	43.58±0.36	
40%	AMFMN	TGRS'22	2.83±0.16	12.65±0.62	23.14±0.85	2.62±0.05	11.76±0.31	21.59±0.31	12.43±0.33
	HVSA	TGRS'23	0.14±0.19	0.62±0.84	1.20±1.67	0.14±0.22	0.65±0.98	1.23±1.73	0.66±0.94
	KAMCL	TGRS'23	2.58±0.91	11.99±3.34	21.16±5.77	3.25±0.48	13.90±1.58	24.13±2.44	12.84±2.27
	SWAN	ICMR'23	1.90±0.20	8.95±0.53	16.89±0.78	2.03±0.06	9.56±0.09	17.98±0.24	9.55±0.23
	PIR	ACMMM'23	6.19±0.70	25.50±0.74	41.58±1.09	5.03±0.05	19.98±0.17	33.91±0.18	22.03±0.43
	S-CLIP	NeurIPS'23	1.92±0.22	9.04±0.74	16.47±1.17	2.13±0.09	9.63±0.51	17.75±1.17	9.49±0.61
	SIRS	TGRS'24	2.27±0.13	10.40±0.26	18.75±0.66	2.10±0.06	9.84±0.19	18.52±0.22	10.31±0.24
	MSA	TGRS'24	2.10±0.19	9.27±0.72	17.34±1.05	2.12±0.11	9.82±0.35	18.75±0.45	9.90±0.34
	SEMICLIP	ICLR'25	4.47±0.23	13.01±0.37	22.44±0.46	3.16±0.23	13.27±0.19	23.14±0.33	13.25±0.16
	CUP	TNNLS'25	8.28±0.80	27.11±2.80	41.52±3.80	4.87±0.62	17.79±1.70	29.69±2.42	21.54±1.98
RRSITR	Ours	20.55±0.32	53.89±0.63	71.10±0.53	12.56±0.16	36.67±0.17	52.51±0.45	41.21±0.19	
60%	AMFMN	TGRS'22	2.15±0.12	9.12±0.76	17.00±1.30	1.94±0.03	9.18±0.14	17.35±0.28	9.46±0.39
	HVSA	TGRS'23	0.04±0.03	0.18±0.03	0.32±0.05	0.03±0.00	0.18±0.02	0.36±0.06	0.19±0.03
	KAMCL	TGRS'23	0.67±0.55	3.07±2.44	6.24±4.97	1.25±0.06	6.25±0.38	11.98±0.89	4.91±1.31
	SWAN	ICMR'23	1.42±0.09	7.47±0.21	14.27±0.36	1.77±0.11	8.47±0.25	15.95±0.36	8.23±0.06
	PIR	ACMMM'23	3.49±0.44	15.90±0.48	27.51±0.86	3.16±0.07	13.26±0.34	23.85±0.58	14.53±0.40
	S-CLIP	NeurIPS'23	0.14±0.06	0.75±0.30	1.36±0.45	0.13±0.06	0.69±0.26	1.28±0.45	0.73±0.25
	SIRS	TGRS'24	1.90±0.13	8.84±0.27	16.41±0.28	1.92±0.11	8.80±0.29	16.64±0.21	9.09±0.12
	MSA	TGRS'24	0.08±0.06	0.54±0.24	1.09±0.40	1.66±0.20	7.75±0.59	14.72±0.89	4.31±0.25
	SEMICLIP	ICLR'25	2.96±0.26	9.12±0.37	15.64±0.63	2.04±0.12	8.96±0.42	16.08±0.77	9.13±0.35
	CUP	TNNLS'25	5.94±0.76	20.05±1.33	32.16±2.34	3.58±0.36	13.91±1.48	23.90±2.07	16.59±1.34
RRSITR	Ours	18.22±0.36	49.11±0.92	66.58±0.80	11.19±0.19	34.13±0.37	49.76±0.35	38.17±0.44	
80%	AMFMN	TGRS'22	1.45±0.18	7.42±0.31	14.47±0.70	1.69±0.10	8.06±0.15	15.43±0.24	8.09±0.19
	HVSA	TGRS'23	0.02±0.02	0.19±0.07	0.34±0.13	0.04±0.01	0.16±0.03	0.34±0.05	0.18±0.03
	KAMCL	TGRS'23	0.02±0.01	0.12±0.03	0.27±0.04	0.02±0.01	0.17±0.01	0.31±0.01	0.15±0.01
	SWAN	ICMR'23	0.79±0.17	4.50±0.30	9.16±0.54	1.00±0.13	5.32±0.37	10.47±0.36	5.21±0.21
	PIR	ACMMM'23	1.70±0.25	7.83±0.44	15.25±0.64	1.44±0.03	7.03±0.12	13.91±0.32	7.86±0.19
	S-CLIP	NeurIPS'23	0.02±0.01	0.17±0.01	0.32±0.00	0.03±0.00	0.17±0.01	0.33±0.01	0.17±0.00
	SIRS	TGRS'24	1.35±0.13	6.77±0.24	12.83±0.25	1.39±0.01	6.50±0.11	12.33±0.28	6.86±0.13
	MSA	TGRS'24	0.02±0.02	0.20±0.04	0.36±0.04	0.52±0.10	2.24±0.44	4.09±0.79	1.24±0.21
	SEMICLIP	ICLR'25	0.94±0.12	3.28±0.46	5.96±0.76	0.78±0.23	3.59±0.49	6.36±0.70	3.49±0.43
	CUP	TNNLS'25	3.87±0.29	14.50±1.23	24.26±1.76	2.35±0.17	9.95±0.59	18.30±0.90	12.21±0.72
RRSITR	Ours	14.94±0.46	41.24±0.54	57.25±0.72	8.75±0.10	28.03±0.21	42.59±0.34	32.13±0.30	

Table 4. Ablation studies on RSITMD with 80% noise ratio.

Method	Image-to-Text Retrieval			Text-to-Image Retrieval			mR
	R@1	R@5	R@10	R@1	R@5	R@10	
#1	15.44	31.64	45.49	11.99	38.13	57.57	33.38
#2	12.08	27.79	39.42	10.29	35.47	53.73	29.80
#3	13.94	29.20	40.66	11.96	34.84	50.64	30.21
#4	13.76	30.22	43.36	11.88	37.50	56.72	32.24
#5	0.18	0.97	1.64	0.36	1.42	2.76	1.22
#6	10.58	25.31	36.11	9.36	31.22	46.53	26.52
#7	0.22	0.79	1.73	0.22	1.20	2.41	1.10
#8	15.09	32.96	45.49	12.82	39.45	57.58	33.90
RRSITR	16.90	33.98	46.82	13.72	42.70	61.47	35.93

loss and the robust triplet loss, thereby ensuring stable and superior performance under varying data quality conditions.

5. Conclusion

This paper studies a challenging problem of Noisy Correspondence (NC) in RSITR, where mismatched image-text pairs are inevitably introduced into the training data, thereby leading to significant performance degradation. To address this issue, we propose a novel Robust Remote Sensing Image-Text Retrieval (RRSITR) paradigm. Specifi-

cally, our RRSITR first categorizes training samples into clean, ambiguous, and noisy pairs through fine-grained alignment. Then, we design a new self-paced learning function to progressively learn reliable image-text correspondences from easy to hard pairs by dynamically assessing the learning difficulty/reliability. Moreover, a robust triplet loss with dynamic soft margins is presented to reduce the negative influence of noisy pairs. Extensive experiments demonstrate that our proposed RRSITR could deal with NC and achieve superior performance compared to state-of-the-art methods under various noise rates.

Acknowledgments This work was supported in part by the National Natural Science Fund of China (Grant No. 62401204), the Hunan Provincial Natural Science Foundation of China under (Grant No. 2026JJ60221), the Sichuan Science and Technology Planning Project (Grant No. 2026NSFSC1480), the MoE Key Laboratory of Brain-inspired Intelligent Perception and Cognition, the University of Science and Technology of China, and the Open Project Program of the State Key Laboratory of CAD&CG Zhejiang University (Grant No. A2512).

References

- [1] Xiumei Chen, Xiangtao Zheng, and Xiaoqiang Lu. Context-aware local–global semantic alignment for remote sensing image–text retrieval. *IEEE Transactions on Geoscience and Remote Sensing*, 63:1–12, 2025. 2
- [2] Qimin Cheng, Haiyan Huang, Yuan Xu, Yuzhuo Zhou, Huanying Li, and Zhongyuan Wang. Nwpu-captions dataset and mlca-net for remote sensing image captioning. *IEEE Transactions on Geoscience and Remote Sensing*, 60:1–19, 2022. 5
- [3] Mehdi Cherti, Romain Beaumont, Ross Wightman, Mitchell Wortsman, Gabriel Ilharco, Cade Gordon, Christoph Schuhmann, Ludwig Schmidt, and Jenia Jitsev. Reproducible scaling laws for contrastive language-image learning. In *Proceedings of the IEEE/CVF Conference on Computer Vision and Pattern Recognition*, pages 2818–2829, 2023. 5
- [4] Haiwen Diao, Ying Zhang, Lin Ma, and Huchuan Lu. Similarity reasoning and filtration for image-text matching. In *Proceedings of the AAAI Conference on Artificial Intelligence*, pages 1218–1226, 2021. 4
- [5] Fartash Faghri, David J Fleet, Jamie Ryan Kiros, and Sanja Fidler. Vse++: Improving visual-semantic embeddings with hard negatives. *arXiv:1707.05612*, 2017. 4
- [6] Kai Gan, Bo Ye, Min-Ling Zhang, and Tong Wei. Semi-supervised CLIP adaptation by enforcing semantic and trapezoidal consistency. In *The Thirteenth International Conference on Learning Representations*, 2025. 2, 5
- [7] Yadong Huo, Qibing Qin, Wenfeng Zhang, Lei Huang, and Jie Nie. Deep hierarchy-aware proxy hashing with self-paced learning for cross-modal retrieval. *IEEE Transactions on Knowledge and Data Engineering*, 36(11):5926–5939, 2024. 3
- [8] Zhong Ji, Changxu Meng, Yan Zhang, Yanwei Pang, and Xuelong Li. Knowledge-aided momentum contrastive learning for remote-sensing image text retrieval. *IEEE Transactions on Geoscience and Remote Sensing*, 61:1–13, 2023. 2, 5
- [9] Zhong Ji, Changxu Meng, Yan Zhang, Haoran Wang, Yanwei Pang, and Jungong Han. Eliminate before align: A remote sensing image-text retrieval framework with keyword explicit reasoning. In *Proceedings of the 32nd ACM International Conference on Multimedia*, pages 1662–1671, 2024. 2, 3
- [10] Karen E Joyce, Stella E Belliss, Sergey V Samsonov, Stephen J McNeill, and Phil J Glassey. A review of the status of satellite remote sensing and image processing techniques for mapping natural hazards and disasters. *Progress in Physical Geography*, 33(2):183–207, 2009. 1
- [11] Diederik P. Kingma and Jimmy Ba. Adam: A method for stochastic optimization. In *3rd International Conference on Learning Representations, ICLR 2015, San Diego, CA, USA, May 7-9, 2015, Conference Track Proceedings*, 2015. 5
- [12] M. Kumar, Benjamin Packer, and Daphne Koller. Self-paced learning for latent variable models. In *Advances in Neural Information Processing Systems*. Curran Associates, Inc., 2010. 2
- [13] Kuang-Huei Lee, Xi Chen, Gang Hua, Houdong Hu, and Xiaodong He. Stacked cross attention for image-text matching. In *Proceedings of the European Conference on Computer Vision*, pages 201–216, 2018. 4
- [14] Jun Li, Yanqiu Pei, Shaohua Zhao, Rulin Xiao, Xiao Sang, and Chengye Zhang. A review of remote sensing for environmental monitoring in china. *Remote Sensing*, 12(7):1130, 2020. 1
- [15] Yansheng Li, Jiayi Ma, and Yongjun Zhang. Image retrieval from remote sensing big data: A survey. *Information Fusion*, 67:94–115, 2021. 1
- [16] Jian Liang, Zhihang Li, Dong Cao, Ran He, and Jingdong Wang. Self-paced cross-modal subspace matching. In *Proceedings of the 39th International ACM SIGIR Conference on Research and Development in Information Retrieval*, pages 569–578, 2016. 2
- [17] Fan Liu, Delong Chen, Zhangqingyun Guan, Xiacong Zhou, Jiale Zhu, Qiaolin Ye, Liyong Fu, and Jun Zhou. Remoteclip: A vision language foundation model for remote sensing. *IEEE Transactions on Geoscience and Remote Sensing*, 62:1–16, 2024. 1, 2
- [18] Xiaoqiang Lu, Binqiang Wang, Xiangtao Zheng, and Xuelong Li. Exploring models and data for remote sensing image caption generation. *IEEE Transactions on Geoscience and Remote Sensing*, 56(4):2183–2195, 2017. 5
- [19] Georgii Mikriukov, Mahdyar Ravanbakhsh, and Begüm Demir. An unsupervised cross-modal hashing method robust to noisy training image-text correspondences in remote sensing. In *2022 IEEE International Conference on Image Processing*, pages 2556–2560. IEEE, 2022. 2
- [20] Sangwoo Mo, Minkyu Kim, Kyungmin Lee, and Jinwoo Shin. S-clip: Semi-supervised vision-language learning using few specialist captions. In *Advances in Neural Information Processing Systems*, pages 61187–61212. Curran Associates, Inc., 2023. 5
- [21] Aaron van den Oord, Yazhe Li, and Oriol Vinyals. Representation learning with contrastive predictive coding. *arXiv preprint arXiv:1807.03748*, 2018. 3
- [22] Jiancheng Pan, Qing Ma, and Cong Bai. A prior instruction representation framework for remote sensing image-text retrieval. In *Proceedings of the 31st ACM International Conference on Multimedia*, pages 611–620, 2023. 2, 5
- [23] Jiancheng Pan, Qing Ma, and Cong Bai. Reducing semantic confusion: Scene-aware aggregation network for remote sensing cross-modal retrieval. In *Proceedings of the 2023 ACM International Conference on Multimedia Retrieval*, pages 398–406, 2023. 2, 5
- [24] Zhengxin Pan, Fangyu Wu, and Bailing Zhang. Fine-grained image-text matching by cross-modal hard aligning network. In *Proceedings of the IEEE/CVF Conference on Computer Vision and Pattern Recognition*, pages 19275–19284, 2023. 4
- [25] Ruitao Pu, Yuan Sun, Yang Qin, Zhenwen Ren, Xiaomin Song, Huiming Zheng, and Dezhong Peng. Robust self-paced hashing for cross-modal retrieval with noisy labels. In *Proceedings of the AAAI Conference on Artificial Intelligence*, pages 19969–19977, 2025. 3

- [26] Yuan Sun, Jian Dai, Zhenwen Ren, Yingke Chen, Dezhong Peng, and Peng Hu. Dual self-paced cross-modal hashing. In *Proceedings of the AAAI Conference on Artificial Intelligence*, pages 15184–15192, 2024. 3
- [27] Xu Tang, Yijing Wang, Jingjing Ma, Xiangrong Zhang, Fang Liu, and Licheng Jiao. Interacting-enhancing feature transformer for cross-modal remote-sensing image and text retrieval. *IEEE Transactions on Geoscience and Remote Sensing*, 61:1–15, 2023. 2
- [28] Xu Tang, Dabiao Huang, Jingjing Ma, Xiangrong Zhang, Fang Liu, and Licheng Jiao. Prior-experience-based vision-language model for remote sensing image-text retrieval. *IEEE Transactions on Geoscience and Remote Sensing*, 62:1–13, 2024. 1
- [29] Yijing Wang, Xu Tang, Jingjing Ma, Xiangrong Zhang, Fang Liu, and Licheng Jiao. Cross-modal remote sensing image-text retrieval via context and uncertainty-aware prompt. *IEEE Transactions on Neural Networks and Learning Systems*, 36(6):11384–11398, 2025. 2, 5
- [30] Jiwei Wei, Xing Xu, Zheng Wang, and Guoqing Wang. Meta self-paced learning for cross-modal matching. In *Proceedings of the 29th ACM International Conference on Multimedia*, pages 3835–3843, 2021. 3
- [31] Dongqing Wu, Huihui Li, Yinxuan Hou, Cuili Xu, Gong Cheng, Lei Guo, and Hang Liu. Spatial-channel attention transformer with pseudo regions for remote sensing image-text retrieval. *IEEE Transactions on Geoscience and Remote Sensing*, 62:1–15, 2024. 1
- [32] Yinghui Xiao and Qingming Zhan. A review of remote sensing applications in urban planning and management in china. In *2009 Joint Urban Remote Sensing Event*, pages 1–5, 2009. 1
- [33] Rui Yang, Shuang Wang, Yingping Han, Yuanheng Li, Dong Zhao, Dou Quan, Yanhe Guo, Licheng Jiao, and Zhi Yang. Transcending fusion: A multiscale alignment method for remote sensing image-text retrieval. *IEEE Transactions on Geoscience and Remote Sensing*, 62:1–17, 2024. 1, 5
- [34] Yuan Yuan, Yang Zhan, and Zhitong Xiong. Parameter-efficient transfer learning for remote sensing image-text retrieval. *IEEE Transactions on Geoscience and Remote Sensing*, 61:1–14, 2023. 1
- [35] Zhiqiang Yuan, Wenkai Zhang, Kun Fu, Xuan Li, Chubo Deng, Hongqi Wang, and Xian Sun. Exploring a fine-grained multiscale method for cross-modal remote sensing image retrieval. *IEEE Transactions on Geoscience and Remote Sensing*, 60:1–19, 2022. 2, 5
- [36] Zhiqiang Yuan, Wenkai Zhang, Xuee Rong, Xuan Li, Jialiang Chen, Hongqi Wang, Kun Fu, and Xian Sun. A lightweight multi-scale crossmodal text-image retrieval method in remote sensing. *IEEE Transactions on Geoscience and Remote Sensing*, 60:1–19, 2022. 1
- [37] Zhiqiang Yuan, Wenkai Zhang, Changyuan Tian, Xuee Rong, Zhengyuan Zhang, Hongqi Wang, Kun Fu, and Xian Sun. Remote sensing cross-modal text-image retrieval based on global and local information. *IEEE Transactions on Geoscience and Remote Sensing*, 60:1–16, 2022. 1
- [38] Kun Zhang, Zhendong Mao, Quan Wang, and Yongdong Zhang. Negative-aware attention framework for image-text matching. In *Proceedings of the IEEE/CVF Conference on Computer Vision and Pattern Recognition*, pages 15661–15670, 2022. 4
- [39] Weihang Zhang, Jihao Li, Shuoke Li, Jialiang Chen, Wenkai Zhang, Xin Gao, and Xian Sun. Hypersphere-based remote sensing cross-modal text-image retrieval via curriculum learning. *IEEE Transactions on Geoscience and Remote Sensing*, 61:1–15, 2023. 2, 5
- [40] Zilun Zhang, Tiancheng Zhao, Yulong Guo, and Jianwei Yin. Rs5m and georsclip: A large-scale vision-language dataset and a large vision-language model for remote sensing. *IEEE Transactions on Geoscience and Remote Sensing*, 62:1–23, 2024. 2
- [41] Chengyu Zheng, Ning Song, Ruoyu Zhang, Lei Huang, Zhiqiang Wei, and Jie Nie. Scale-semantic joint decoupling network for image-text retrieval in remote sensing. *ACM Transactions on Multimedia Computing, Communications and Applications*, 20(1):1–20, 2023. 1
- [42] Wenqian Zhou, Hanlin Wu, and Pei Deng. Toward efficient and accurate remote sensing image-text retrieval with a coarse-to-fine approach. *IEEE Geoscience and Remote Sensing Letters*, 22:1–5, 2025. 1
- [43] Zicong Zhu, Jian Kang, Wenhui Diao, Yingchao Feng, Junxi Li, and Jingen Ni. Sirs: Multitask joint learning for remote sensing foreground-entity image-text retrieval. *IEEE Transactions on Geoscience and Remote Sensing*, 62:1–15, 2024. 1, 2, 5